THE ASDEX 100 keV NEUTRAL LITHIUM BEAM DIAGNOSTIC GUN

K. McCormick, M. Kick

IPP III/85 April 1983

MAX-PLANCK-INSTITUT FÜR PLASMAPHYSIK

8046 GARCHING BEI MÜNCHEN

MAX-PLANCK-INSTITUT FÜR PLASMAPHYSIK

GARCHING BEI MÜNCHEN

THE ASDEX 100 keV NEUTRAL LITHIUM BEAM DIAGNOSTIC GUN

K. McCormick, M. Kick

IPP III/85 April 1983

Die nachstehende Arbeit wurde im Rahmen des Vertrages zwischen dem Max-Planck-Institut für Plasmaphysik und der Europäischen Atomgemeinschaft über die Zusammenarbeit auf dem Gebiete der Plasmaphysik durchgeführt.

Table of Contents

IPP III/85 K. McCormick
M. Kick

THE ASDEX 100 keV NEUTRAL LITHIUM BEAM DIAGNOSTIC GUN

April 1983
(in English)

Abstract

The neutral lithium beam gun intended for measurement of the poloidal magnetic field and of the density gradient in the scrape-off layer of ASDEX is described, and test results over a beam energy range of 27 - 100 keV are presented. In the gun, lithium ions are extracted from a solid emitter (ß-Eucryptite) in a Pierce-type configuration, accelerated and focused in a two-tube immersion lens, and neutralized in a charge-exchange cell using sodium. The beam can be pulsed from less than one to several seconds, depending on experimental needs. At a distance of 165 cm from the gun the neutral beam equivalent current is typically greater than 1 mA (0.16 mA) for a beam energy of 100 keV (27 keV), the beam FWHM being about 8 - 9 mm. It is found that to produce a particular beam width a certain ratio must be maintained between the extraction and total beam voltages, this relationship depending in turn on the emitter-extractor separation.

The principal features which distinguish the ASDEX gun from that employed on W7a /1/ are the greater compactness - all the active elements, i.e. emitter, extractor, lens, deflection plates and neutralizer, are contained within 57 cm - and the vacuum vessel, which simultaneously serves as the magnetic shielding.

List of Symbols

$D_{1/2}$	Beam FWHM
ε'	Apparent beam neutralization efficiency = I_d^o/I_d
ε	Beam neutralization efficiency = $(1+\gamma/\varepsilon'+\gamma)\ \varepsilon'$
γ	Secondary electron emission coefficient
I_e	Emitter current (power supply current)
I_b	Total beam current = $I_b^+ + I_b^o$
I_b^+	Beam ion current
I_b^o	Beam neutral equivalent current
I_d	Detector current resulting from total beam = $\gamma I_b + I_b^+$
I_d^+	Detector current resulting from beam ions = I_b^+
I_d^o	Detector current resulting from beam neutrals = γI_b^o
$L_{e\text{-}ext}$	Separation between emitter and extractor
L_{lens}	Separation between the tubes forming the lens
V_b	Beam voltage
V_{ext}	Extraction voltage

1. Introduction

Successful measurements of the poloidal magnetic field on the Pulsator tokamak at low densities using a 6 keV, 10 μA neutral lithium beam demonstrated the feasibility of the Zeeman spectroscopic technique /2/, but also made clear that higher beam energies /3/ and currents were necessary in order to extend the diagnostic operating range to higher densities and larger experiments. The 100 keV, 1 mA neutral lithium beam gun subsequently developed for W7a /1/ could not be used on ASDEX due to the higher stray magnetic fields and the more restrictive geometry of ASDEX, thereby necessitating the design of a new gun predicated upon the W7a version. This report describes salient mechanical features of the ASDEX gun, and documents its operating characteristics in a beam energy range of 27 - 100 keV as determined on a test setup relevant to ASDEX conditions. The mid-range energies are of interest mainly for the measurement of the density gradient in the scrape-off layer (proof-of-principle experiment, reference /4/), whereas the higher energies should find application in the determination of the poloidal magnetic field.

2. The Neutral Lithium Beam Gun

The ASDEX gun is shown in the to-scale schematic of Fig. 1. It consists of an emitter, an extractor, a two-tube lens to accelerate and focus the ions, an accel-decel aperture ("electrostatic barrier aperture") which prevents electrons in the beam from entering the lens region, a set of x-y deflection plates, and a charge-exchange cell in which the beam is neutralized. The system is necessarily compact due to geometrical restrictions on ASDEX imposed by the presence of a neutral beam injector box and the spatial variation of the stray magnetic field.

2.1 Mechanical Layout

As can be seen in Figures 1 and 2a, the vacuum vessel is made of three parts: the emitter-extractor-tube section; the middle piece containing the grounded lens tube, the electrostatic barrier aperture and the x-y deflection plates; and the neutralizer housing.

The emitter-extractor-tube complex, which lies at high potential (emitter: beam voltage, extractor-tube: beam voltage minus the extraction voltage), is connected to the middle piece via a ceramic insulator, and is contained within a pressure vessel filled with SF_6 to prevent sparking to adjacent structures. At an SF_6 pressure of three Bar the hold-off voltage is determined to be greater than 120 kV.

For purposes of beam optimization the emitter-extractor separation is variable via a bellows, which is shown in Fig. 2b - with the HV shielding removed - along with the insulator. In order to adjust the lens focal length, the spacing between the two tubes is also adjustable: Fig. 2c shows the middle section with the grounded tube. The x-y deflection plates, intended for moderate corrections to the beam trajectory, are to be seen in Fig. 2d: the plates are situated in the same plane as a result of the requirement that the gun be as short as possible.

The neutralizer housing is cooled, and is separated from the middle section by a baffle which serves to optically limit the amount of sodium deposited in the ion gun by the neutralizer as well as to provide a differential pumping stage between ASDEX and the high voltage region of the gun. (The neutralizer is not mounted in Fig. 2a.)

Operation of ASDEX at its maximum parameters leads to a stray magnetic field of about 360 gauss in the vicinity of the neutralizer housing, falling off to about 200 G at the start of the SF_6 pressure vessel. The vacuum- and SF_6-vessels

are made of ARMCO iron (plated with 15μ of nickel to protect against rust and establish more favorable vacuum properties) in order to shield against these fields. Independent tests with cylinders indicated that if the magnetic field within the iron is kept below 6 kG then the field in the shielded region will be less than one gauss. The necessary thickness t to achieve this situation, for the case of a cylinder whose axis is perpendicular to an incident magnetic field of magnitude B, is given by /5/

$$t \simeq D \frac{B}{6} \frac{[kG]}{kG} \qquad (1)$$

where D is the outer diameter of the cylinder. Using formula (1) and others appropriate to the gun geometry /6/ one sees that the (~20 mm thick) vacuum vessel walls should provide more than adequate shielding - which has been verified by actual operation on ASDEX. To compensate for the somewhat higher fields (~10 kG for max. ASDEX parameters) within the 6 mm pressure vessel walls, a second shield consisting of a 1 mm thick cylinder of μ-metal is used. A 90^{o} pumping elbow and a collar (both not shown in Fig. 2a) made of ARMCO are employed to reduce field penetration through the pump ports. All ARMCO parts are heat treated to enhance magnetic properties.

Two Leybold Turbovac 150 turbopumps produce a vacuum in the 10^{-7} - 10^{-6} mbar range when the gun is in operation.

2.2 The Emitter and Ion Optics

The emitter is a heavy-duty version of the standard 600 ion source of Spectra-Mat, Inc. (Watsonville, Calif.) coated with the lithium aluminosilicate, ß-Eucryptite ($Li_2O \cdot Al_2O_3 \cdot 2SiO_2$) /7/. When heated to a temperature of about 1400 ^{o}C (power consumption $\lesssim$ 200 W) and an electric field is applied, lithium ion currents of several mA can be extracted from the surface of approximately 1.7 cm^2 area. For a description of the ion

source, the coating procedure and some operational characteristics, see reference /1/. A picture of the mounted ion source is shown in Fig. 3a.

The layout of the emitter-extractor and of the lens, and the associated dimensions shown in Fig. 1 were determined - largely empirically - during the development of the W7a gun and are discussed in reference /1/. Here, the only differences to the W7a version lie in the increased mechanical stability of the moveable components and in the shortening of the 30 mm diameter tube from 100 to 65 mm. Figure 3b is a picture of the emitter-extractor-tube complex with the HV shield in place. (The HV shield as well as the SF_6 vessel are beveled so as to avoid mechanical conflict with the neutral beam injector box on ASDEX).

In testing the W7a gun it was discovered that the current drawn from the HV power supplies could be reduced by applying a negative voltage to one of the deflection plates and grounding the opposite plate. Based upon the suspicion that this net negative voltage was acting as a potential barrier to electrons downstream in the beam, preventing them from accelerating to the emitter and producing secondary electrons, an accel-decel aperture was installed with the hope of duplicating this effect. The run-in phase of the ASDEX gun subsequently demonstrated that this "electrostatic barrier aperture" was indeed effective in reducing the current (apparently) extracted from the emitter.

2.3 The Neutralizer

The charge-exchange cell used for neutralizing the lithium ion beam consists of a neutralization tube, of 2.4 cm inner diameter and 12 cm length, attached to a reservoir which supplies the neutralizing medium, either lithium or sodium. To reduce cell losses operation is on a pulsed basis by

means of a pneumatically driven valve which seals the reservoir during periods when the beam is not on. For most of the measurements reported here the cell was heated to temperatures such that the neutralization efficiencies for a Li^+ beam on sodium ranged from about 92 % at 27 keV to more than 50 % at 100 keV.

Details concerning the design, mechanical layout and efficacy of the charge-exchange cell are to be found in reference /8/.

3. The Experimental Test Layout

The test layout is depicted in Fig. 4. It is made up of the lithium beam gun and four beam detectors arranged at distances relevant to the ASDEX geometry. The magnet is used to deflect ions from the beam in order to measure the efficiency of the charge-exchange cell.

The scannable Faraday cup (SFC), with an entrance aperture of 3 mm diameter, and the swing probe - consisting of a molybdenum rod of 3 mm diameter - are used to scan the beam profile on a shot-to-shot basis. The SFC is intended for use on ASDEX in the geometry shown in Fig. 4. The swing probe is meant to model a molybdenum rod probe fixed within the ASDEX vacuum vessel. Both probes are included in the layout primarily for calibration purposes.

3.1 The Beam Profile Monitor

In the test series discussed in section 4 most profile information is won with the rotating-mirror beam profile monitor (RMBPM) which is placed at a distance of 164 cm from the neutralizer. A schematic of the setup is shown in

the insert of Fig. 4: the slit image (width ~3 mm) is scanned across the beam by a rotating mirror. Light from the lithium resonance line at 6708 Å - which is excited via interaction of the lithium beam atoms with the background gas - is registered by a photomultiplier after having passed through a broad band interference filter. Two tungsten lamps which are also included in the scan serve to spatially calibrate the oscillograph trace of the PM output. In order to be able to increase the background gas pressure - thereby increasing the light intensity - in the region of examination without unduly raising the pressure in the entire beam line, the interaction chamber is somewhat decoupled from the main vacuum vessel by means of two long tubes of 30 mm inner diameter. In practice the general background pressure ($\sim 10^{-6}$ - 10^{-5} mbar) resulting from the beam-Faraday cup interaction was more than adequate to produce good signals.

The advantages of the RMBPM compared to a normal rotating wire monitor operating on a secondary electron emission basis lie in the facts that the method is sensitive only to beam neutrals, and that the measured (chord) profile is precisely that which is of interest when the beam is to be used for a spectroscopic diagnostic.

3.2 The Faraday Cup

The Faraday cup (FC), situated about 198 cm from the neutralizer, measures the ion I_b^+ and equivalent neutral beam I_b^o currents passing through the 30 mm diameter entrance aperture. Referring to Fig. 4, for the case of a Faraday cup configuration where the outer cylinder is grounded, the collector plate and inner cylinder are connected, and the middle cylinder is biased at a negative voltage sufficient to suppress secondary electrons, the detector current I_d^+ is equal to I_b^+. Conversely, by connecting the two inner cylinders and biasing them at a

positive voltage, the detector registers the current of secondary electrons released from the collector $\gamma(I_b^{\,o} + I_b^{\,+})$ as well as the ion current $I_b^{\,+}$.

The secondary electron emission coefficient γ is taken to be equal for ions and neutrals, and is determined by comparing the beam ion current $(I_d^{\,+})$ to the corresponding secondary electron current $(\gamma I_b^{\,+})$. For the collector used, a molybdenum plate oriented at a 45^o angle to the beam, γ is found to have a dependence on the beam voltage V_b $(27 \leq V_b \leq 100$ kV) given by

$$\gamma \simeq 0.018\ V_b\ [\text{kV}] + 3.56 \qquad (2)$$

4. Gun Test Results

4.1 Preliminary Remarks

The test series documented here had two main goals:

a) to verify that the gun functioned properly, and b) to gain some feeling for the parametric dependence of the total beam current I_b $(I_b^{\,o} + I_b^{\,+})$ and beam FWHM $D_{1/2}$ on the beam voltage V_b, extraction voltage V_{ext}, emitter current I_e, and the emitter-extraction separation $L_{e\text{-}ext}$ within the context of an ASDEX-oriented application. No attempt per se was made to categorize beam properties in a more general sense.

All measurements are carried out with the charge-exchange cell activated. Hence I_b can be determined only indirectly. However, it is easy to show that when the FC is operated in the secondary electron emission mode, I_b is related to the detector current I_d by

$$I_b = \frac{\varepsilon' + \gamma}{1 + \gamma}\ \frac{I_d}{\gamma} \qquad (3)$$

where ε' is the apparent neutralization efficiency defined as

$$\varepsilon' = \frac{I_d^{\,o}}{I_d} = \frac{\gamma I_b^{\,o}}{\gamma I_b + I_b^{\,+}} \tag{4}$$

which is the ratio of the detector currents $I_d^{\,o}$ ($\gamma I_b^{\,o}$) due only to beam neutrals to the detector current I_d ($\gamma I_b + I_b^{\,+}$) arising from the total beam. In other words, $I_d^{\,o}$ and I_d represent the detector signals with the beam deflection magnet turned on and off, respectively.

With respect to the effectiveness of the charge-exchange cell, the beam neutralization efficiency ε is given by

$$\varepsilon = \frac{I_b^{\,o}}{I_b^{\,o} + I_b^{\,+}} = \frac{I_b^{\,o}}{I_b} = \left(\frac{1+\gamma}{\varepsilon' + \gamma}\right)\varepsilon' \ . \tag{5}$$

The variation of ε' and ε with lithium beam energy for a particular charge-exchange cell power setting is shown in Fig. 10.

The emitter current increases with beam voltage. In order that the emitter not be too rapidly depleted of lithium ions most parametric investigations were conducted at the (moderate) beam energy of about 54 keV. Less systematic checks at other energies served to verify the generality of the behavior patterns ascertained at 54 keV.

Again to avoid lithium ion depletion of the emitter the high voltage was pulsed on for only one second; longer shots of many seconds are possible by simply extending the length of the high voltage pulse. The emitter was continuously heated at a power level (<200 W) appropriate to space-charge-limited extraction conditions, i.e. the power was increased to the point where the extraction voltage alone determined I_e. Deviation from this state leads to results different from those summarized in Figures 5 to 9.

Biasing the electrostatic barrier aperture to about -400 V proved sufficient to suppress excessive (apparent) emitter currents. Still higher voltages tended to slightly defocus the beam, particularly for lower beam energies.

4.2 Results

Figure 5a shows four profiles of the beam light intensity taken with the RMBPM for extraction voltages ranging from 5 to 5.5 kV; the lens voltage is held constant at 48 kV and $L_{e\text{-}ext}$ = 19 mm. The beam FWHM $D_{1/2}$, as deduced from the profiles is plotted vs. V_{ext}/V_b in Fig. 5b, and the associated valves for the total beam current I_b and emitter current I_e are indicated in Fig. 5c. We see that increasing V_{ext} leads to broader profiles (~ 7 - 13 mm) and higher beam currents (~0.5 - 0.8 mA: through the 30 mm aperture of the FC). In addition the fraction I_b/I_e of the emitter current which appears in the detected portion of the beam increases from about 25 to 35 %.(Note that the "emitter current" - HV power supply current - may have a contribution due to secondary electrons.) It is seen that the profile shape is not constant; rather, the base remains roughly the same with the central part of the beam being filled out as V_{ext} is increased. (The 30 mm diameter baffle tubes attached to the RMBPM interaction chamber establish the width of the base). Figure 5b illustrates the precision with which V_{ext} must be controlled to maintain a particular beam width: for instance, around $D_{1/2}$ = 8 mm, a ±2 % change (~100 V) in V_{ext} alters $D_{1/2}$ by ~±1.2 mm.

For E_b = 53.2 keV and $L_{e\text{-}ext}$ = 19 mm the effects of varying the separation L_{lens} between the two tubes forming the lens on $D_{1/2}$ and I_b are shown in Fig. 6. Adjusting L_{lens} between 91 and 67 mm leads to an increase in $D_{1/2}$ from 8 to 11.5 mm and an associated decrease in the beam current entering the detector from 0.61 to 0.44 mA. Sporadic point checks for higher beam energies and larger $L_{e\text{-}ext}$ revealed a similar

but less sensitive dependence of $D_{1/2}$ and I_b on L_{lens}. Consequently L_{lens} was left at a setting of 88 mm.

These results are in contrast to those found in reference /1/. There the detector current reached a maximum for L_{lens} = 66 mm. It is not clear if the different behavior can possibly be attributed to the smaller emitter-extractor separation ($L_{e\text{-}ext}$ = 16 mm), the higher beam energy of 97 keV, or the rather high (for $L_{e\text{-}ext}$ = 16 mm) ratio V_{ext}/V_b of 0.102. The facts that the detector had a fixed position and sampled only a portion of the beam could lead in any case to different results if, for example, the beam center shifted slightly as L_{lens} was changed.

Figures 7a and 7b show the variation of $D_{1/2}$, I_b, I_e and I_b/I_e as a function of V_{ext}/V_b for $L_{e\text{-}ext}$ = 23 mm. While the trends are the same as for the $L_{e\text{-}ext}$ = 19 mm case of Fig. 5, $D_{1/2}$ increases somewhat more sharply with V_{ext}/V_b, I_b and I_e are now only a weak function of V_{ext}/V_b, and I_b/I_e is in the range 34 - 38 %. Furthermore, the increase in $L_{e\text{-}ext}$ has led to an increase in the value of V_{ext}/V_b necessary to produce a certain beam width: this behavior is quantified in Fig. 8a where the value of V_{ext}/V_b necessary to produce a beam of width 9 mm is plotted against $L_{e\text{-}ext}$. Although this plot is for a beam energy of 54 keV, the curve is applicable for all beam energies. Likewise, the variation of $D_{1/2}$ with V_{ext}/V_b for a particular $L_{e\text{-}ext}$ is approximately given by Fig. 7a, using Fig. 8a to calibrate V_{ext}/V_b for $D_{1/2}$ = 9 mm.

Figure 8b shows that I_b has a broad maximum around $L_{e\text{-}ext}$ = 22 mm, and that I_e decreases with increasing $L_{e\text{-}ext}$ leading to a maximum value of I_b/I_e of ~38 % at $L_{e\text{-}ext}$ = 25 mm. Evidently if the highest possible beam current is not of primary importance, it is desireable to operate at a large emitter-extractor separation thereby reducing I_e and prolonging the emitter life. An accompanying side effect to

larger $L_{e\text{-}ext}$ is a marked reduction in the frequency of voltage breakdown between the emitter and extractor.

The dependence of I_b, I_b^o, I_e and I_b/I_e on lithium beam energy is shown in Fig. 9 for which $L_{e\text{-}ext}$ = 24 mm. V_{ext}/V_b is adjusted so as to maintain a beam width of 8-9 mm. I_b is roughly proportional to the square of the beam voltage, ranging from ~ 0.19 mA at 27 keV to ~ 2.1 mA at 100 keV. I_e goes from 1.8 to 4.5 mA, yielding an I_b/I_e increasing from 23 to 45 % respectively, i.e. higher beam energies allow a more efficient use of the extracted emitter current.

It should be emphasized that the I_b curve of Fig. 9a does not represent the maximum value of I_b attainable as a function of energy. In accordance with Figures 7 and 8b an increase in V_{ext}/V_b ($\rightarrow$ larger $D_{1/2}$) and/or a decrease in $L_{e\text{-}ext}$ will lead to a moderate improvement.

In Fig. 9a I_b^o tends to flatten out at higher energies because of the decreasing beam neutralization efficiency ε (plotted in Fig. 10). Above ~ 80 keV the beam atom density actually slightly decreases! As described in reference /8/, ε can be augmented somewhat by raising the temperature of the charge-exchange cell.

5. Summary and Conclusions

The direct coupling of the emitter-extractor configuration to a two-tube lens arrangement which both accelerates and focuses the ion beam leads to a very compact system (distance: emitter/end of lens tube ~28 cm), but necessitates that a precisely defined relationship be maintained between the extraction and total beam voltages, and the

emitter-extractor separation in order to form a well-collimated beam. Thus, when $L_{e\text{-}ext}$ = 24 mm, then $V_{ext}/V_b \sim .107$ to produce a beam FWHM of 9 mm at a distance of 164 cm from the gun. The sensitivity of the beam parameters to V_{ext}/V_b is exemplified by the fact that a ±2 % change in V_{ext} noticeably affects both the beam current (~+4% - 8 %) and beam FWHM (~ +35 % - 18 %). Further, since the emitter current increases with the extraction voltage, higher beam voltages automatically imply higher beam currents: $I_b(I_b^o)$ varies from ~0.19 mA (0.16 mA) at 27 keV to ~2.1 mA ($\gtrsim$1 mA) at 100 keV, for $D_{1/2}$ = 8 - 9 mm. The ratio I_b/I_e changes from 23 to 45 %, respectively.

Within the limits investigated here the emitter-extractor separation does not appear to be of principal importance: the extraction voltage can always be adjusted accordingly to achieve a particular beam width. An $L_{e\text{-}ext}$ of ~23 mm seems to be a reasonable compromise between the goals to maximize beam strength and to minimize emitter current. However, when the emitter becomes so depleted of lithium ions that I_e is emission limited, i.e. not space-charge limited, then the variable $L_{e\text{-}ext}$ feature is useful in re-optimizing the beam in accordance with the changed extraction conditions.

Finally, although beam properties near to the gun were not examined in any detail, it was found that at a distance of 64 cm from the neutralizer the beam FWHM could be brought below 4 mm.

Acknowledgements

I thank Mr. H. Schmid and Miss H. Sittig for assisting in setting up the test layout.

References

/1/ M. Kick, K. McCormick and H. Schmid, IPP Report 2/265 (Jan. 1983).

/2/ K. McCormick, M. Kick and J. Olivain, 8th Eur. Conf. on Contr. Fusion and Plasma Physics, Prague (1977) 40.

/3/ K. McCormick, IPP Report III/40 (January 1978).

/4/ K. Kadota, K. Tsuchida, Y. Kawasumi and J. Fujita, Plasma Physics 20 (1978) 1011.

/5/ A.J. Mager, IEEE Trans. on Magnetics, Vol. MAG-6, No.1 (March 1970) 67.

/6/ Firmenschrift FS-M9, Magnetische Abschirmungen, Vacuumschmelze GmbH, Hanau (1975).

/7/ J.P. Blewett and E.J. Jones, Phys. Rev. 50 (1936) 464.

/8/ K.McCormick, IPP Report III/82 (March 1983).

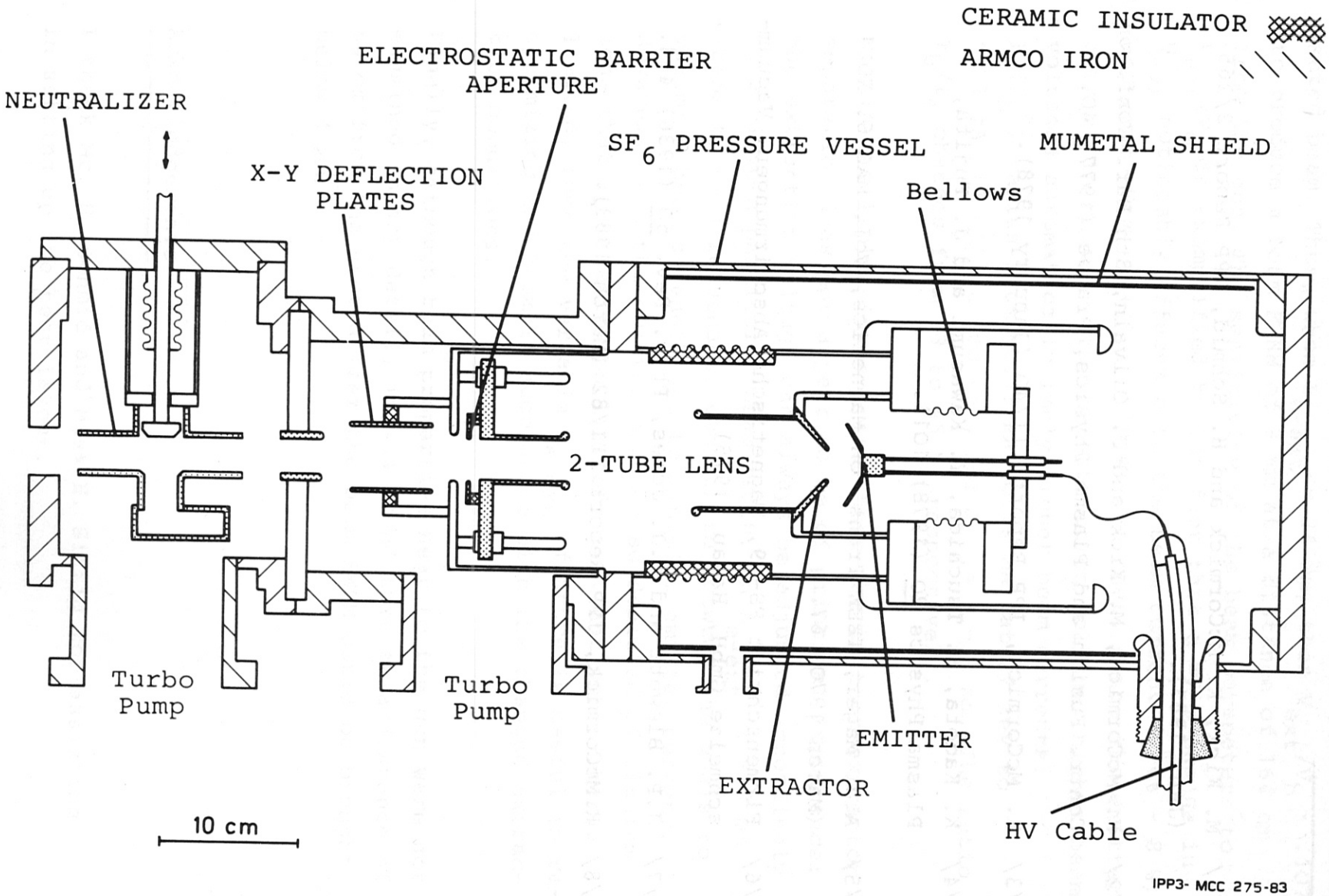

Fig. 1 Simplified drawing of the ASDEX lithium ion gun with neutralizer

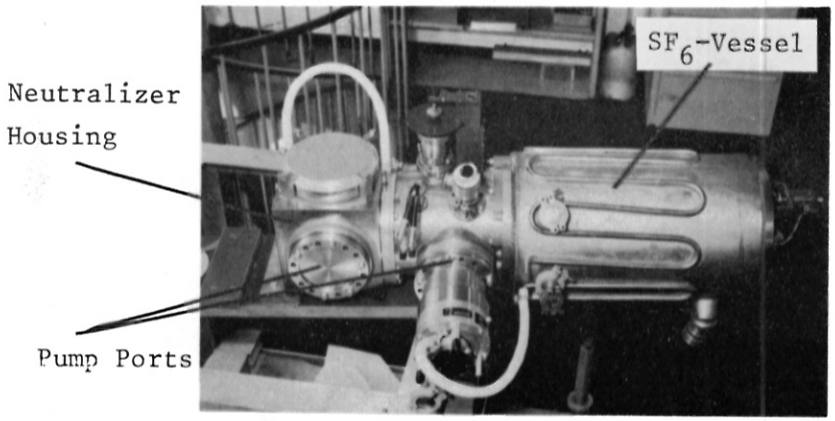

Fig. 2a The ASDEX neutral lithium beam gun

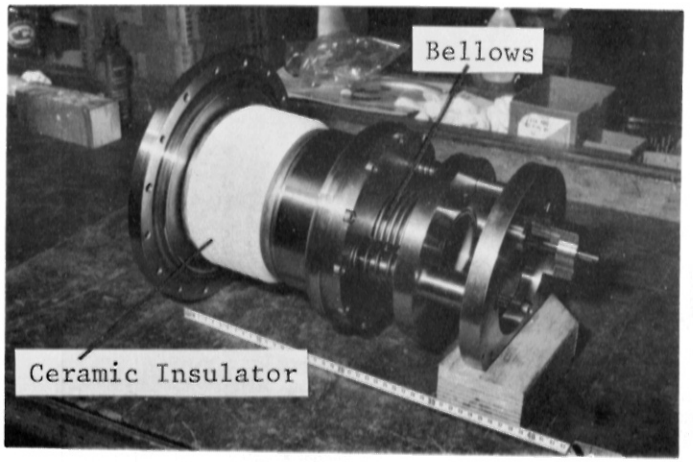

Fig. 2b HV insulator with bellows for adjusting emitter-extractor separation

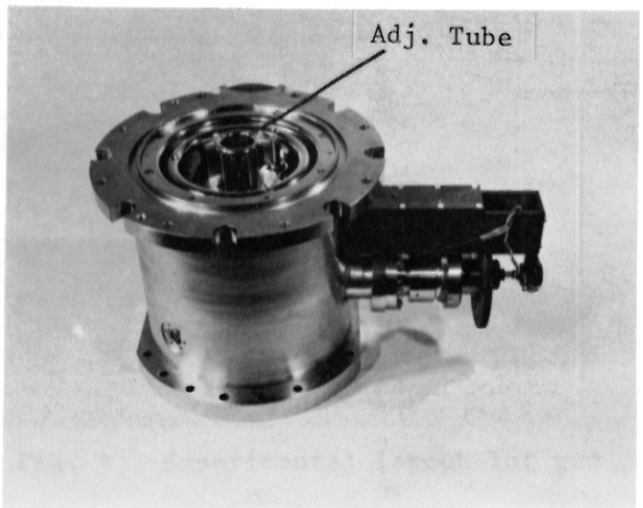

Fig. 2c Middle section: adjustable tube

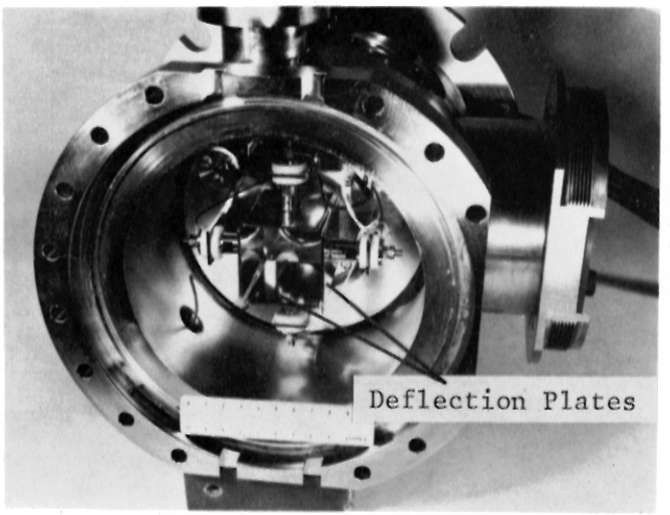

Fig. 2d Middle section: deflection plates

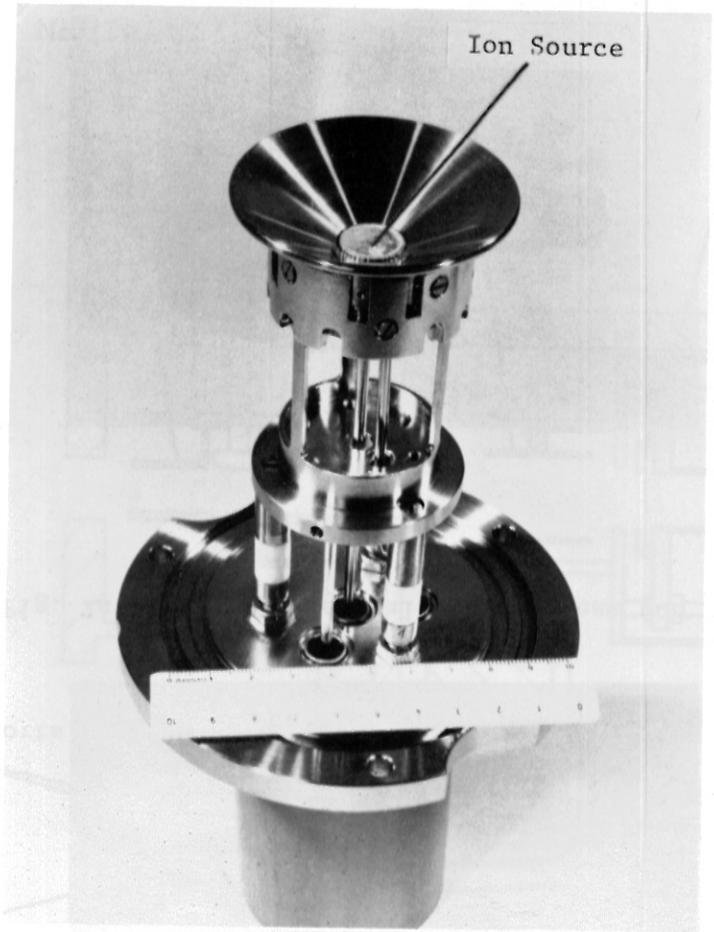

Fig. 3a Holder for Spectra-Mat ion source

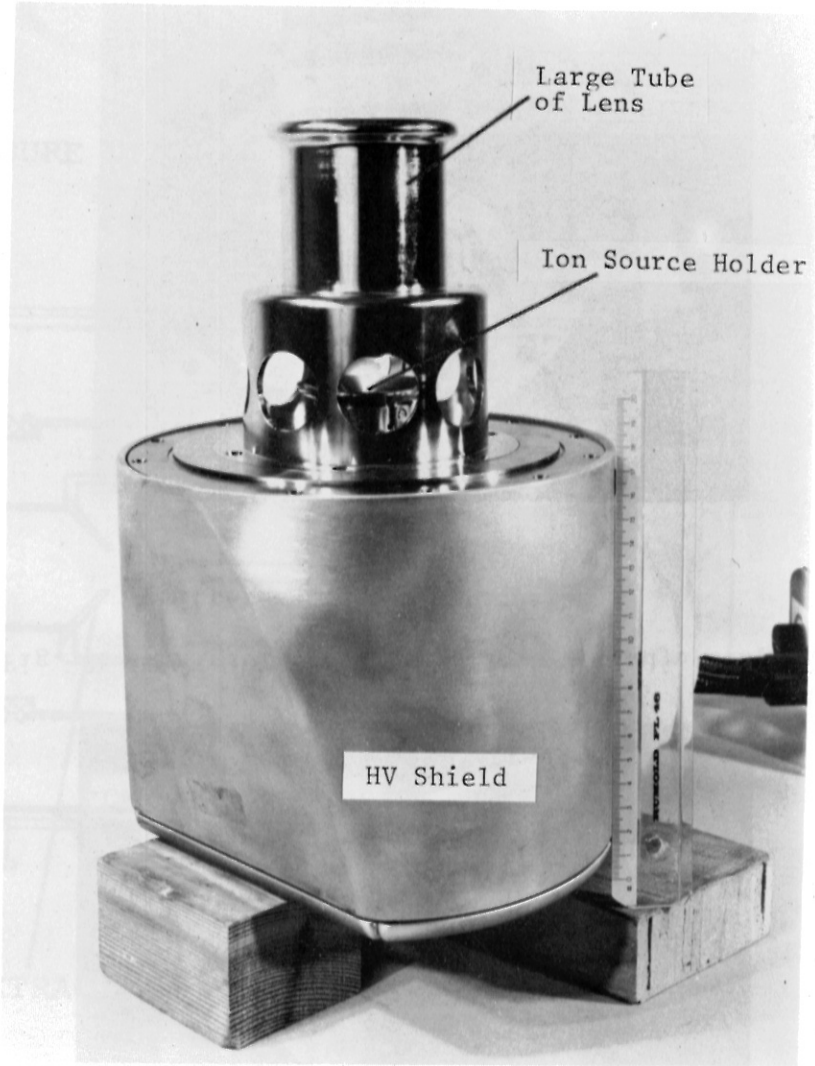

Fig. 3b Ion source with extractor and one lens tube

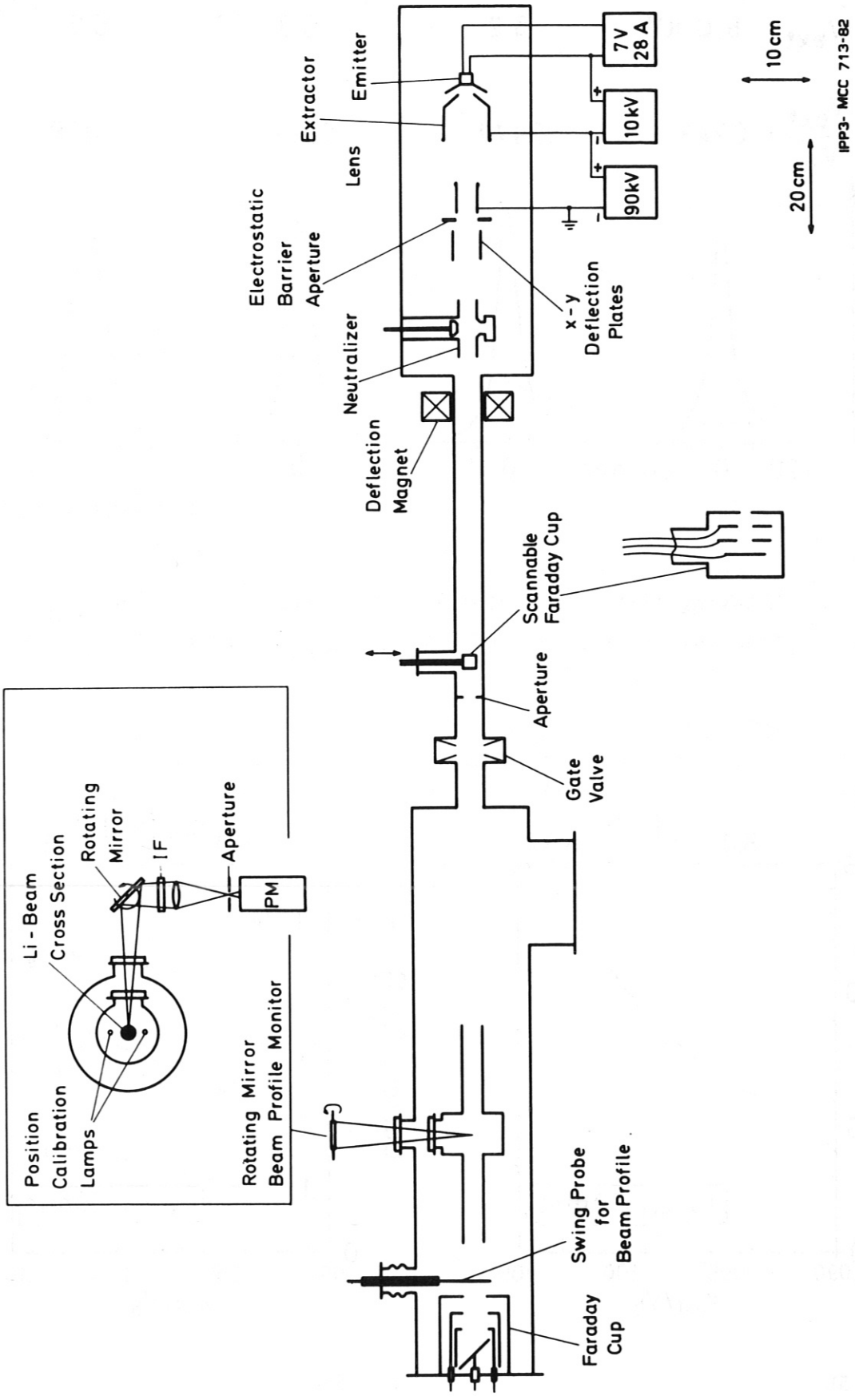

Fig. 4 Experimental layout for gun tests

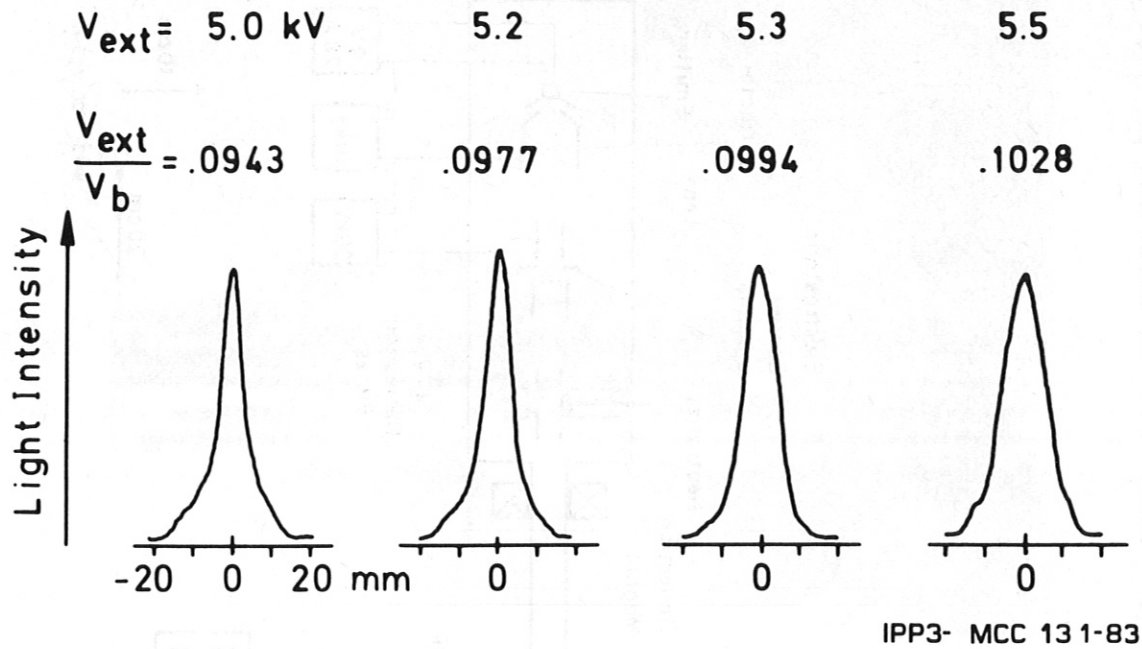

Fig. 5a Rotating mirror beam profiles vs. extraction voltage V_{ext}. Beam voltage V_b[kV] = 48 + V_{ext}, $L_{e\text{-}ext}$ = 19 mm, L_{lens} = 88 mm.

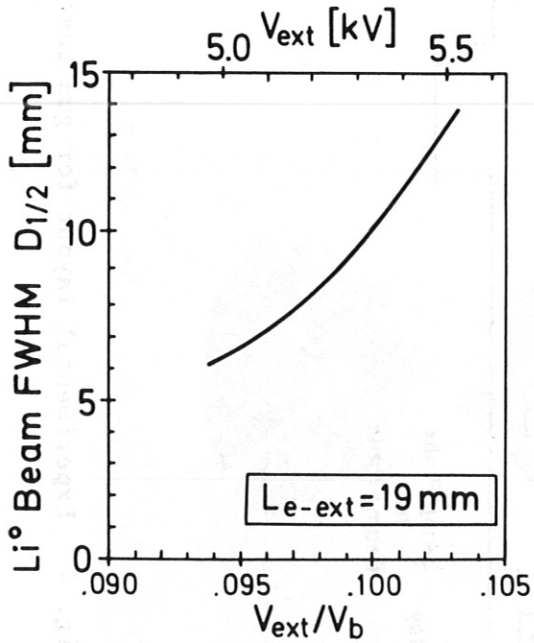

Fig. 5b

Li° beam FWHM $D_{1/2}$ vs. V_{ext}/V_b

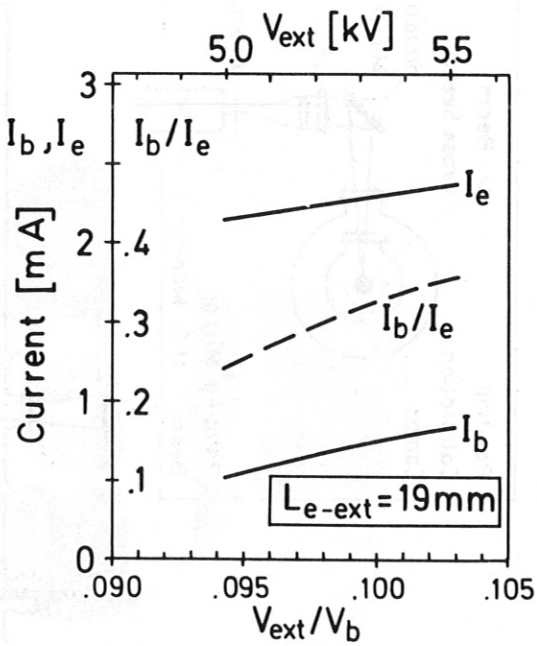

Fig. 5c

Total Li beam current I_b, emitter current I_e and I_b/I_e vs. V_{ext}/V_b

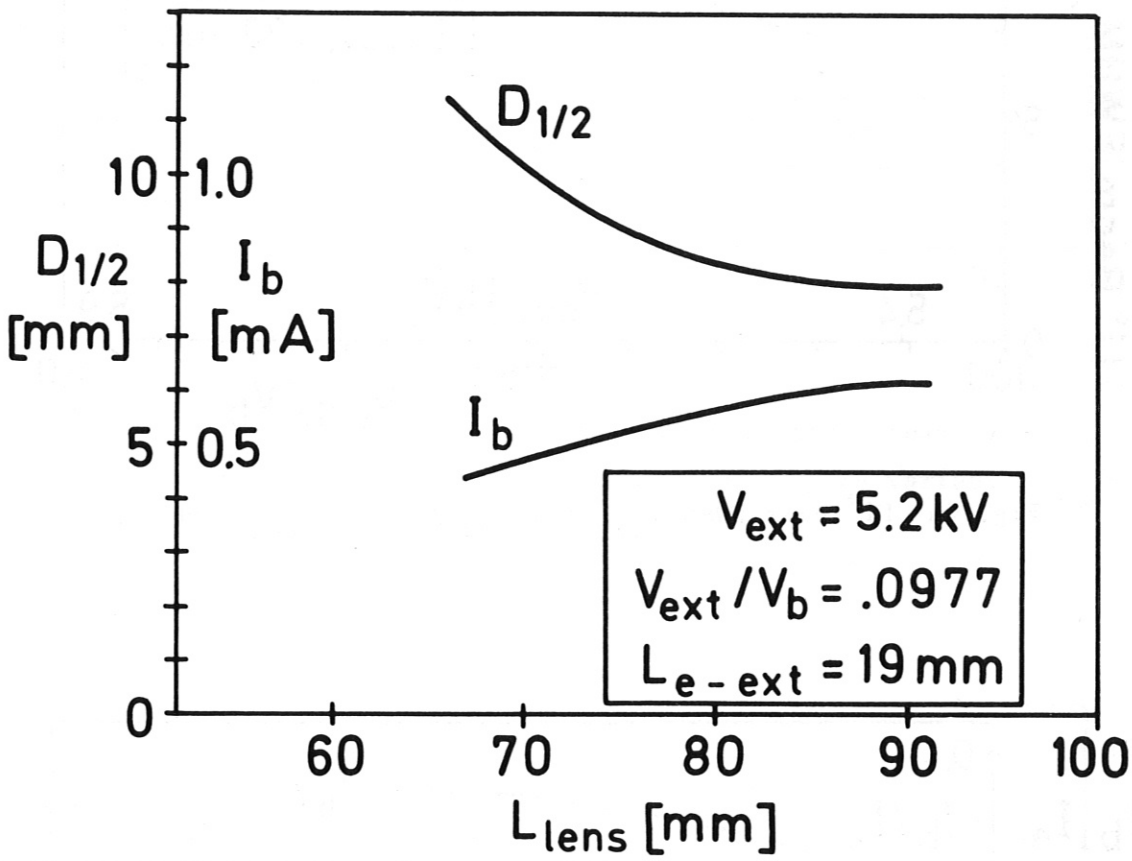

Fig. 6

Li^{o} beam FWHM $D_{1/2}$ and total beam current I_b vs. lens tube separation L_{lens}

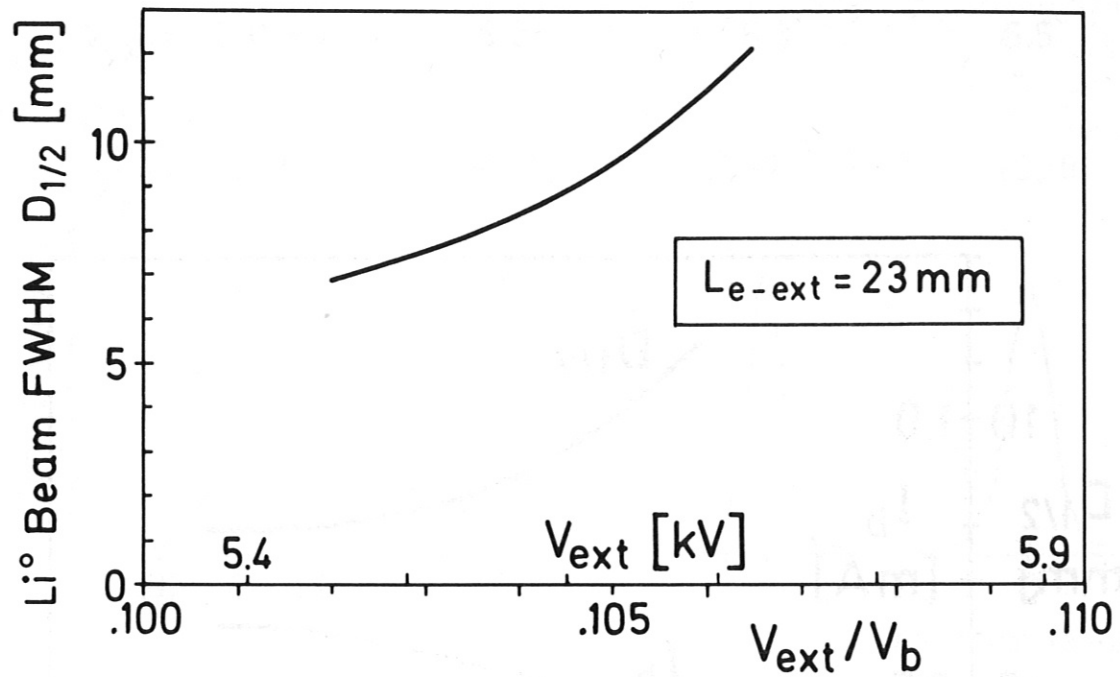

Fig. 7a Li^{o} beam FWHM $D_{1/2}$ vs. V_{ext}/V_b. L_{lens} = 88 mm

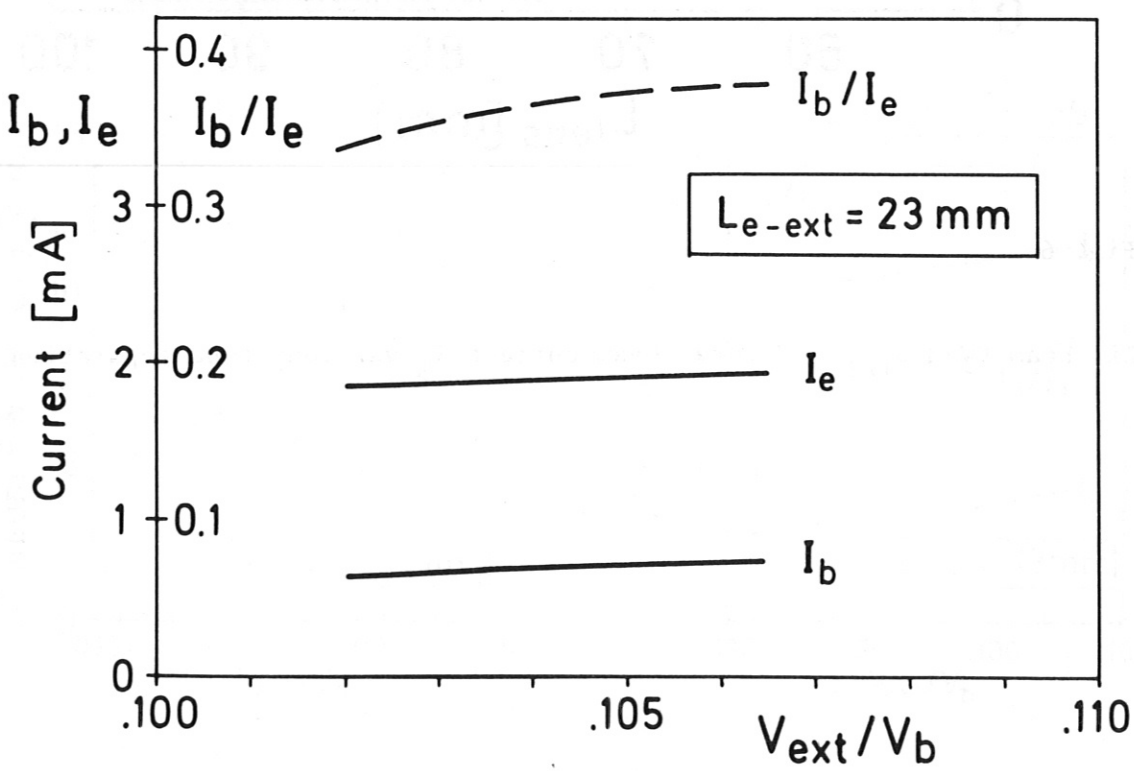

Fig. 7b Total Li beam current I_b, emitter current I_e and I_b/I_e vs. V_{ext}/V_b

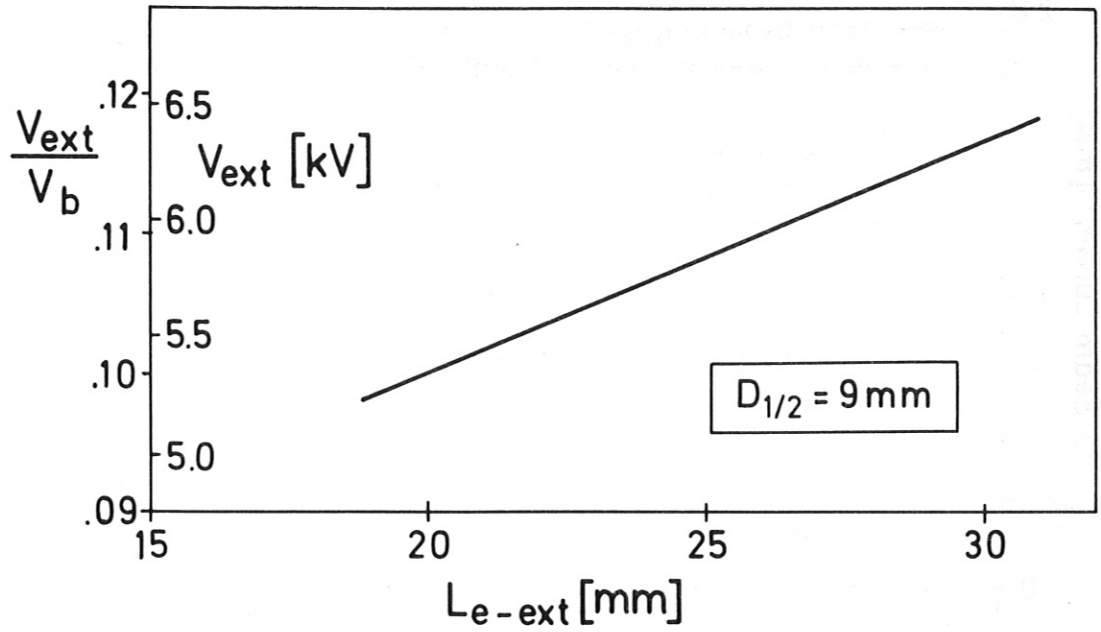

Fig. 8a Value of the ratio V_{ext}/V_b necessary to maintain a beam FWHM of 9 mm as the emitter-extractor separation $L_{e\text{-}ext}$ is varied. $L_{lens} = 88$ mm

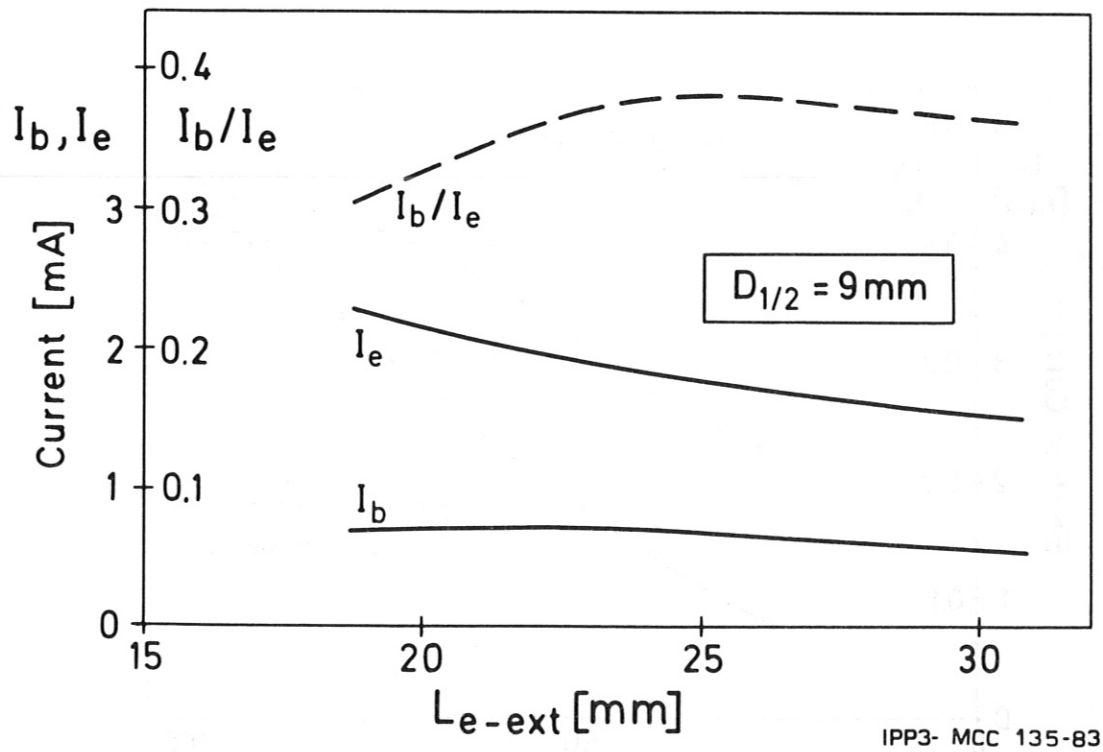

Fig. 8b Total Li beam current I_b, emitter current I_e and I_b/I_e vs. $L_{e\text{-}ext}$ for the values of V_{ext}/V_b indicated in Fig. 8a

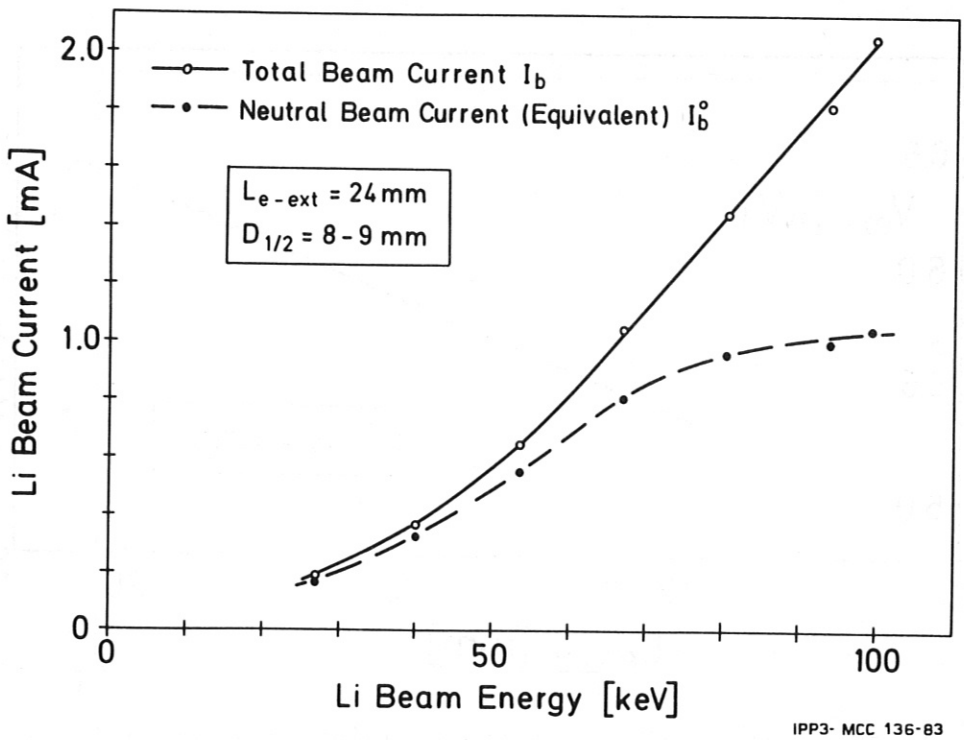

Fig. 9a Total beam current I_b and neutral beam current I^o_b vs. Li beam energy. V_{ext}/V_b is adjusted so as to maintain $D_{1/2}$ = 8 - 9 mm. L_{lens} = 88 mm

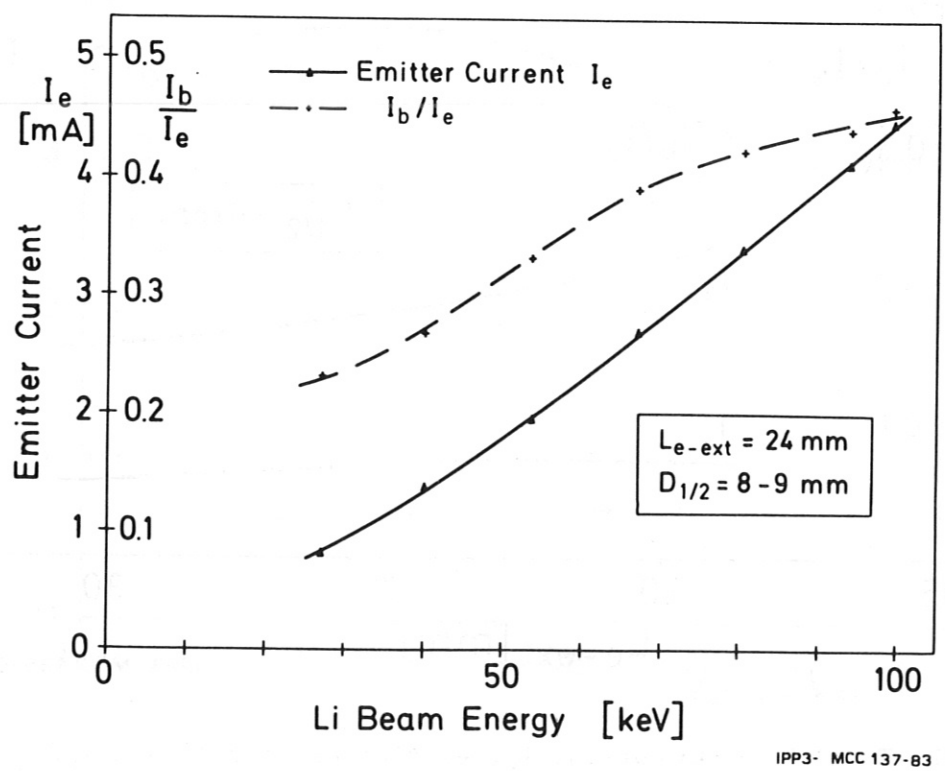

Fig. 9b Emitter current I_e and I_b/I_e associated with the beam currents of Fig. 9a vs. Li beam energy

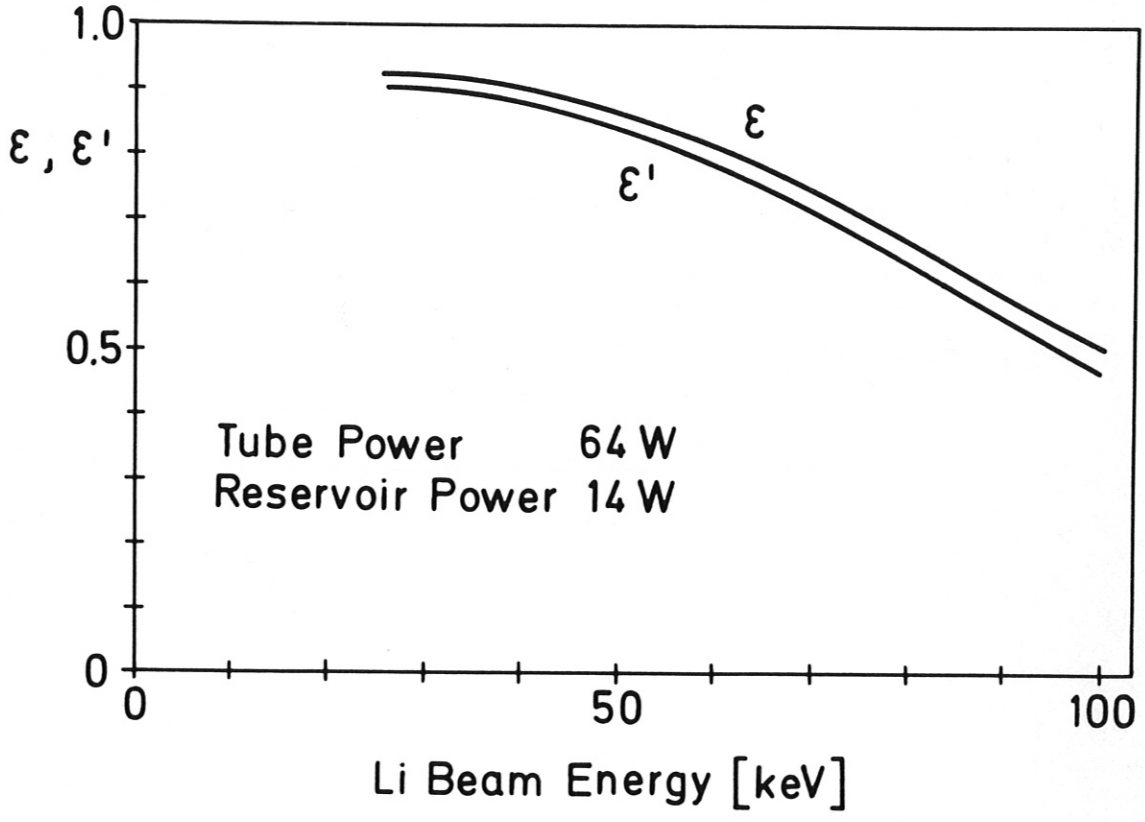

Fig. 10 The apparent and actual beam neutralization efficiencies, ε' and ε respectively, vs. Li beam energy for the charge-exchange cell power settings used for Fig. 9.